Height, structure and displacements of noctilucent clouds

By GEORG WITT, *Institute of Meteorology, University of Stockholm.*

(Manuscript received October 2, 1961)

ABSTRACT

Observations of noctilucent clouds have been carried out during the summer of 1958 at Torsta (63.3° N ; 14.6° E) in Central Sweden as part of the IGY working program of the Institute of Meteorology, University of Stockholm. Simultaneous pairs of cloud photographs have been taken with accurate phototheodolite cameras from the end-points of a geodetically determined base-line of length 51.5 km. The picture pairs were subsequently analyzed in stereo instruments (autographs) by which Cartesian space coordinates were obtained for various points in the cloud system. These coordinates, duly corrected for atmospheric refraction, were used for determination of the height of the individual features. Through the stereoscopic effect, measurements could be made on diffuse parts of the cloud system as well as on marked details. Additional information about movements of the cloud system was obtained from a time-lapse film in Kodachrome. The results were plotted and analyzed by conventional methods and maps of the cloud topography at consecutive time intervals could be prepared. In addition to these maps, vertical cross-sections through the cloud system were made as well as detailed studies of particularly interesting cloud features. This paper gives a presentation and interpretation of the results obtained so far and a brief description of the photogrammetric technique applied.

The results presented below were obtained during a very bright cloud display with good visibility conditions on August 10–11th, 1958. Thirty pairs of pictures were taken of various parts of the cloud system, which covered the entire northern horizon. Eight of these have been analyzed so far. The results can be summarized as follows. The cloud system moved in a direction north-east to south-west with velocities of the order of 50 to 100 m/s. It consisted of a continuous diffuse layer interchanging with regions of sharply defined features such as systems of parallel billows and bands, blobs and other smaller-scale irregularities of various shapes. The measured heights varied between 81.5 and 85.5 km. The long parallel bands were identified as a system of waves with wavelengths of the order of 50 km and amplitudes up to 4 km which propagated in a direction nearly opposite to that of the cloud system with absolute velocities of the order of 10 to 20 m/s. The wave crests were oriented nearly perpendicular to the main air flow and were continuous over distances of hundreds of kilometers and exhibited local refraction effects. The smaller billows had wavelengths of the order of 5–10 km and amplitudes about 0.5–1.0 km; they moved with the cloud sysem. The billows showed no preferred orientation and were observed to pass through the crests of the longer waves. It is indicated by the analysis the regular changes in the brightness of these clouds are due to changes of the optical thickness of the cloud layer, particularly at the rear slope of the long waves. The measured details had well-defined lower boundaries.

Introduction

A continued investigation of the nature of noctilucent clouds has been conducted since 1955 at the observing station of the Institute of Meteorology of the University of Stockholm, located at Torsta (63.3° N ; 14.6° E) in Central Sweden (Ludlam, 1957; Witt, 1957). The working program has included (*a*) visual cloud observations from Torsta with associated observing stations in Scandinavia and in Greenland, the network being shown in Fig. 1, (*b*) measurements of the polarization of the light scattered by the clouds for determination of the size range of the cloud particles and (*c*) the study of the height and structure of the clouds by means of photogrammetric methods. The results from recent photogrammetric measurements are presented and discussed in this paper, the polarization measurements having been described elsewhere (Witt, 1960). A summary of the synoptic visual observations will be published separately.

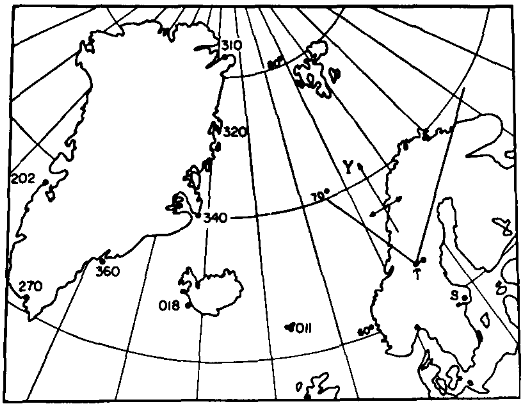

Fig. 1. Network of stations taking part in the noctilucent cloud observational programme. Stockholm is denoted hy *S* and Torsta with associated secondary instrument site is denoted by *T*. The intersecting solid lines indicate the approximate boundaries of the visible part of the cloud system observed on August 10–11, 1958. The horizontal coordinate axes of the reference system used in the photogrammetric height determination are indicated by the intersecting arrows.

Although noctilucent clouds have been regarded as more or less a peculiarity, a systematic study of their specific nature can give useful information concerning the state of the mesosphere region of the upper atmosphere. The technique of high-altitude rocket sounding is today becoming more and more advanced. Still, our best direct indicators of movements at the 80–km level are meteor trails and noctilucent clouds. Whereas the vertical profile of local horizontal wind velocities is best determined from studies of the deformation of meteor, or rocket trails, noctilucent clouds can be expected to give a picture of horizontal changes in the airflow. The unusual height and high velocities of these clouds were first measured by JESSE (1896), and Tserasski and Pokrovski (KHVOSTIKOW, 1952). Jesse has measured the cloud heights from pairs of photographs taken from the end-points of a base-line of length 35 km. The height values were found to vary between 79 and 90 km, the mean of the measured values being about 82 km. The clouds were found to move predominantly from a direction between north and east with velocities up to 100 to 200 m per sec. Similar results were also found by the Russian observers. These early observations have been further confirmed by more recent work first of all by STÖRMER (1935) and by PATON (1949). In Southern Norway, Störmer has established a network of camera stations connected by base-lines of 105, 65 and 47 km which were originally designed for measurement of the height of the polar aurora. Photographs were taken simultaneously from these stations and the heights were computed from the parallax between identical points in corresponding pictures. The parallax was measured in a system of coordinates obtained from photographs of stars into which the pictures were projected. Störmer's individual values varied from 78 to 85 km with mean values between 81 and 82 km. A disadvantage of Störmer's method lies in the difficulty of definition of identical points in photographs of such a diffuse object as noctilucent clouds. Accordingly, the measurements are confined to bright and well-defined cloud features such as waves or billows. A distinct improvement of the photographic method is made by applying the stereoscopic effect. This technique implies simultaneous analysis of both pictures in an analyzing instrument such as a stereocomparator or autograph. (A detailed description of these instruments may be found in standard textbooks on photogrammetry.) Through the stereoscopic effect the portion of the clouds in the field of view is seen in three dimensions. Each eyepiece of the analyzing instrument is fitted with a measuring mark. One of these may be adjusted to cover the particular detail to be measured in the corresponding pictures. The marks appear to the observer as a single point located behind or in front of the measured detail according to the parallax between the pictures. By varying the parallax, the mark is seen to travel with respect to the clouds and the correct reading is made when the mark appears to touch the measured feature. This phenomenon is illustrated by anaglyph pictures in Fig. 2 where the photographic pairs are printed together. The measuring mark is here represented by an arrow. The method permits a good accuracy in the parallax determination. Moreover, the method allows the measurements to be extended to more diffuse parts of the cloud system if the contrast in the pictures is sufficient and if bright features in the surroundings are used as auxiliary points. The method permits a good measuring accuracy provided the base-line is carefully determined, and in order to avoid uncertainty due to a change in position in the clouds, the times of exposure are moderate. Last, but not least, the cameras must be good ballistic cameras with long focal length and large aperture. Based upon these considerations, a series of measurements were carried out at Torsta during the summer 1958. After this work was completed, Burov (1959) published results from similar measurements in the USSR. His height values are consistent with those presented here. The successful accomplishment of this work has been made possible by the generosity of the Bofors Company, which placed a pair of phototheodolites at our disposal, the costs of which otherwise would have been prohibitive. For this we are greatly indebted. We have also to express our thanks to Messrs. Y. Lehman and O. Nyman from the Royal Swedish Artillery for valuable aid in the geodetical survey work; and to Messrs. S. Möller and T. Granér of the Royal Survey Office for their kind cooperation in the analysis of the photographic records.

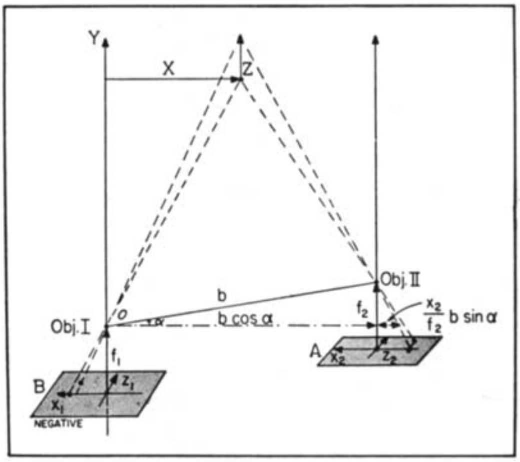

Fig. 3. Geometry of the basic photogrammetric system. The origin of the reference coordinate system is in the centre of projection of camera B, denoted by O. The Y-axis is pointing in the zero direction in the plane tangent to the earth at B. The base is denoted by b and the camera constants by f_1 and f_2. The inclination of the base to the X-axis is due to the fact that the reference directions were determined before the azimuth of the base was known. Notice the increase of the length of base for negative values of x_2.

Basic theory

In the following we shall briefly present the mathematical background to terrestrial photogrammetry as applied to our special purposes. We consider a pair of ballistic cameras located at the endpoints A and B of a base-line of lenth b (see Fig. 3). Point B is located to the west from A. The centre of projection of camera B is selected as the reference point O. This point is the origin of a right-handed Cartesian coordinate system in the plane tangent to the earth at O. The horizontal Y axis is the zero direction which is parallel to the zero direction of the local map projection system. Due to the convergence of meridians the zero direction deviates slightly from true north. The Z coordinate is measured vertically upward.

Let us first consider the case when the optical axes of the two cameras are mutually parallel and directed perpendicularly to the base-line. We refer to this as the normal-parallel case. The geometry of the system may be seen in Fig. 3 if the angle $\alpha = 0$. A point (Y,X,Z) has corresponding image coordinates B (f_1, x_1, z_1) and A (f_2, x_2, z_2), the pictures being viewed in the negative position. Here f_1 and f_2 are the camera constants which are not necessarily equal. The origin of the image coordinate system is defined by the intersection of lines through the fiducial marks in each negative. By geometrical similarity one obtains the basic formulas of terrestrial photogrammetry:

$$Y = b \cdot f_1/P, \tag{1a}$$

$$X = b \cdot x_1/P = Y \cdot x_1/f_1, \tag{1b}$$

$$Z = b \cdot z_1/P = Y \cdot z_1/f_1, \tag{1c}$$

p is the parallax defined by

$$p = x_1 - (f_1/f_2)x_2. \tag{2}$$

The coordinates of the second picture enter only in the expression for the parallax. In practical applications the ideal normal-parallel conditions may be difficult to realize due to any of the following three reasons which, occasionally, as in the Torsta case, occur simultaneously.

(a) The optical axes of the cameras are kept parallel but the zero direction is no longer perpendicular to the base. This case occurs when a zero direction has to be fixed before the azimuth of the base-line is known. The geometry is again seen from Fig. 3. By geometrical similarity we find that the basic formulas

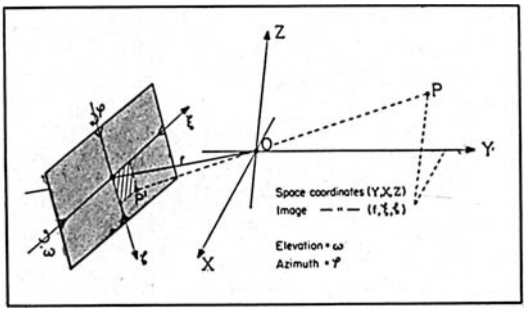

Fig. 4. The figure shows the correspondence between a point in space P (Y, X, Z) and its image P' (f, ξ, ζ) in the case of rotated cameras. The elevation angle is denoted by ω and the azimuth by φ.

(1) are still valid provided the base length b is replaced by the length of the effective base b', as defined by:

$$b' = b \cdot [\cos\alpha - (x_2/f_2)\sin\alpha], \qquad (3)$$

where α denotes the inclination of the X-axis to the base. Thus, the effective base is found to vary from point to point.

(*b*) The limited field of view of the cameras may necessitate a rotation of the instruments in both azimuth and elevation. The parallelity between the optical axes is assumed to be preserved even here. Denote the elevation angle by ω and the azimuth by φ, positive eastward. The coordinates of the rotated negatives are denoted by (f_i, ξ_i, ζ_i), as indicated in Fig. 4. If the rotated coordinates are projected into the normal system (f_i', x_i, z_i) formulas (1) again become applicable. Mathematically the projection can be expressed by the matrix multiplication:

$$\begin{bmatrix} f_i' \\ x_i \\ z_i \end{bmatrix} = \begin{bmatrix} \cos\varphi & -\sin\varphi & 0 \\ \sin\varphi & \cos\varphi & 0 \\ 0 & 0 & 1 \end{bmatrix} \cdot \begin{bmatrix} \cos\omega & 0 & -\sin\omega \\ 0 & 1 & 0 \\ \sin\omega & 0 & \cos\omega \end{bmatrix} \cdot \begin{Bmatrix} f_i \\ \xi \\ \zeta \end{Bmatrix} \qquad (4)$$

The order between the factors should be noticed. A possible rotation $\varkappa$ about the optical axis is neglected, but may be allowed for in a similar way.

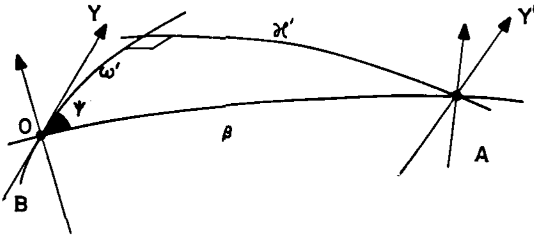

Fig. 5. Corrections for the curvature of the earth along the base line. The arc β and the angle of inclination of the reference direction to the base ψ are determined from a geodetic survey, which also provides the directions Y and Y'. When the base line is inclined to the X-axis, the curvature correction may be performed in two steps, the first of these being a rotation $\varkappa'$ of the secondary image about the Y'-axis and the second a perpendicular rotation ω'. The angles of rotation are found from formulae (6). The corrections have to be made on the normal coordinates after these have been obtained.

(*c*) In the case of long base-lines the cameras must be levelled and centred independently. Parallelity of the optical axes may still be maintained as the individual zero directions are determined from geodetical measurements. The curvature of the earth will, however, cause a convergence of the vertical axes, with a corresponding inclination between the z_1 and z_2 axes. Fortunately the curvature effect can be compensated by a rotation of the local normal coordinate system A about the secondary zero axis. In this way the normal-parallel conditions are again restored. In the case where the zero direction is not perpendicular to the base, the correction has to be performed in two steps. The first step is a rotation of the secondary system about its zero axis and the second about the local X axis. The rotation components are deduced from the spherical triangle in Fig. 5, where the arc β along the base is the hypotenuse. We use again the matrix notation and denote the rotation around the zero axis by $\varkappa'$ and its perpendicular component by ω' as indicated. The reduced normal coordinates of the secondary picture $(f_2, x_2, z_2)_r$ are expressed by:

$$\begin{bmatrix} f_2' \\ x_2 \\ z_2 \end{bmatrix}_r = \begin{bmatrix} \cos\omega' & 0 & \sin\omega' \\ 0 & 1 & 0 \\ -\sin\omega' & 0 & \cos\omega' \end{bmatrix} \cdot$$

$$\cdot\begin{bmatrix}1 & 0 & 0\\ 0 & \cos\varkappa' & \sin\varkappa'\\ 0 & -\sin\varkappa' & \cos\varkappa'\end{bmatrix}\cdot\begin{bmatrix}f_2'\\ x_2\\ z_2\end{bmatrix} \quad (5)$$

Here, $$\sin\varkappa' = \sin\psi\cdot\sin\beta \quad (6)$$
$$\cos\omega' = \cos\beta/\cos\varkappa'$$

and ψ is the measured angle between the zero direction and the base. The measured curvature of the Torsta base-line amounted to 0.465 degrees of arc. Particularly in the case of rotated cameras the magnitude of z frequently exceeds the x-value. It is easily understood that the omission of a term $z\cdot\sin\varkappa'\cdot\cos\omega'$ may give rise to considerable systematic errors, even for fairly small angles.

The numerical conversion of the measured coordinates is a laborious procedure, particularly in the case of a vast number of points. The use of an electronic computer is in such a case advisable. Much of the labour can be eliminated if the pictures are analyzed in a stereo-autograph. Basically this instrument is an analogue computer. The negatives are inserted into the machine in the same relative position as at the instant of exposure. The base-line and optical axes are represented by steel rods and the space coordinates are read directly from a dial on the parallax screw. The path described by the measuring mark can be drawn automatically by a map-drawing apparatus to give contour lines of bright cloud features. Moreover, since the horizontal coordinates are known in advance, the heights can be measured at previously fixed "grid-points" by which a subsequent map analysis is facilitated. We found from experience that points measured in a comparator showed a tendency to accumulate around bright details. Using the autograph this problem can be overcome.

Before the computation of heights H over the surface of the earth the measured Z values must be corrected for atmospheric refraction. This effect is pronounced at low elevation angles, where the clouds are usually observed, and refraction errors may be of the order of a kilometer or more. Since the clouds are located outside the regions of the atmosphere which primarily contribute to refraction, the corrections can be made with the aid of tables of astronomical refraction. In our case the pro-

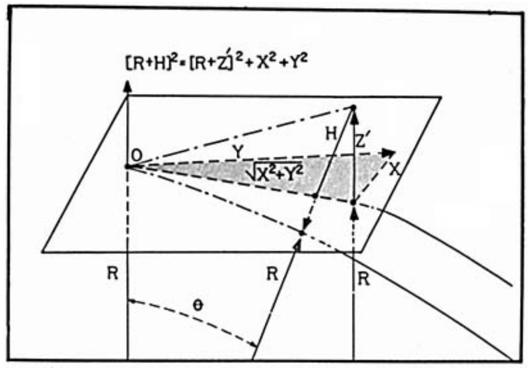

Fig. 6. Computation of the height H above surface level. The coordinates X and Y are as defined before and Z' is the height above the tangent plane corrected for atmospheric refraction. The radius of the earth is denoted by R and Θ is the zenith angle to the point measured. The elevation of the observation point above sea level is here neglected.

cedure has been simple because local meteorological conditions were similar to the normal conditions of the tables used. Any further refinement would have entered as a second order correction and was neglected. The formulae for the computation of the height H are easily deduced from the geometry shown in Fig. 6.

$$(R+H)^2 = (R+Z')^2 + Y^2 + X^2, \quad (7)$$

where R is the radius of the earth assumed spherical and Z' is the corrected height. The spherical distance at cloud level is expressed by

$$S = (R+H)\cdot \text{arc sin}\,(\sqrt{Y^2+X^2}[R+H]). \quad (8)$$

Having presented the mathematical formulae there remains to be discussed the possible random and systematic errors involved in the procedure. It is not our intention to give a systematic analysis of such errors in this paper. An objective determination of systematic errors requires pairs of photographs of known celestial objects taken at exactly known times. Unfortunately, there are few bright stars in the portion of the sky where the clouds are observed. No stars are visible in the analyzed photographs, and due to unfavourable weather conditions following the few clear days of the observation period, no further photographs could be made. The magnitude of random errors arising from the analysis may still be estimated. Assume that errors due to misalignment are negligible, and that all corrections listed above have been duly performed. We consider only the normal-parallel case. By differentiating formulae (1) and (2) followed by some manipulation and neglecting terms containing db and df we obtain:

$$\left.\begin{aligned} \delta Y &= Y^2 \delta p / b \cdot f_1 \\ \delta X &= X \delta Y / Y + Y \delta x_1 / f_1 \\ \delta Z &= Z \delta Y / Y + Y \delta z_1 / f_1 \simeq \delta Z' \\ |\delta H| &= \left\{ \frac{(R+Z')^2 (\delta Z)^2 + Y^2 (\delta Y)^2 + X^2 (\delta Y)^2}{(R+Z')^2 + Y^2 + Y^2} \right\}^{\frac{1}{2}} \end{aligned}\right\} \quad (9)$$

From these formulae the dependence of the accuracy on the focal length and the base-line is clearly seen. It is obvious that the reading accuracy will depend on the contrast and definition of the cloud details. Here we assume a plausible error of ± 0.1 mm in the determination of all image coordinates. This is fairly large compared with the limit of resolution of a common photographic emulsion, about 0.02 mm. Using the data of the Torsta network we find that $|\delta Y| = 1.4$ km, and the uncertainty in the height determination is about ± 350 m for a typical point with $Y = 500$ km, $X = 0$ and $Z =$ 66 km. Since our interest has been turned toward relative differences in the cloud topography rather than an absolute height determination, systematic errors of similar magnitude due to second-order effects have been neglected. Such errors should be expected to cause a mere deformation or inclination of the cloud model on a larger scale.

This section ends with a summary of data and coordinates of the Torsta network. The geodetical coordinates have been determined by triangulation. Angles and directions were defined within an accuracy of 10″. The error in the base-line determination is less than ± 5 m. The position of point A was selected with regard to an open horizon, optimal base length and azimuth, and last but not least, satisfactory conditions for VHF radio communication.

Point B (Torsta)
Longitude: $\lambda_B =$ 14.035°
Latitude: $\Theta_B =$ 63.251°
Elevation: $Z_B = 392.9$ m

Point A (Mårdsjön)
$\lambda_A = 15.502°$
$\Theta_A = 63.282°$
$Z_A = 384.0$ m

Arc $(B - A)$: $\beta = 0.4630°$. The corresponding distance $S = 51{,}510.25$ m. Using these values the effective height difference between the stations becomes $Z = 208.1$ m. The inclination of the X direction to the baesline $\alpha = 3.1496°$. The rotations due to the curvature of the earth are $\varkappa' = 0.4623°$ and $\omega' = 0.0254°$. The earth was assumed to be spherical, with $R = 6375$ km. The constants of the cameras were identical $f_1 = f_2 =$ 378.66 mm. The cameras were Zeiss phototheodolites with Tessar 1:5 objectives and an image size of 13 by 18 cm (Fig. 7). Both instruments have been provided with a device for illumination of the fiducial marks, a necessary aid in night-time operation. Camera data given by the proprietor were accepted. The instruments were mounted on cylindrical iron pedestals set into concrete pads. The exposures were synchronized with the aid of VHF radio communication between the operators. The duration of the exposures varied from 5 to 25 seconds as was determined from experience. Kodak P1200 and O800 plates were used alternatively in order to avoid complete failure due to underexposure in the case of insufficient brightness. The plates were processed conventionally in a Methol-Hydrochinone developer. Certain plates were reduced to half the original size in an accurate reproduction apparatus of the Swedish Cartographic Office in order to make them suitable for autograph analysis. The numerical work following the analysis was made on an electronic computer, and the results were plotted and analyzed by conventional methods.

Results

The photographic equipment described above was set up for operation during the period July 25 to August 15, 1958. The network was first used during a display of noctilucent clouds of moderate brightness on August 5. This time the photographic work was disturbed by tropospheric clouds. Due to an accident, the only result obtained was a series of single pictures. These photographs have not been analyzed so far, although single pictures could also be used for studies of the cloud movements by assuming a mean cloud height. The second display followed on August 10–11 with optimal conditions. Tropospheric clouds were practically absent from the northern horizon and the

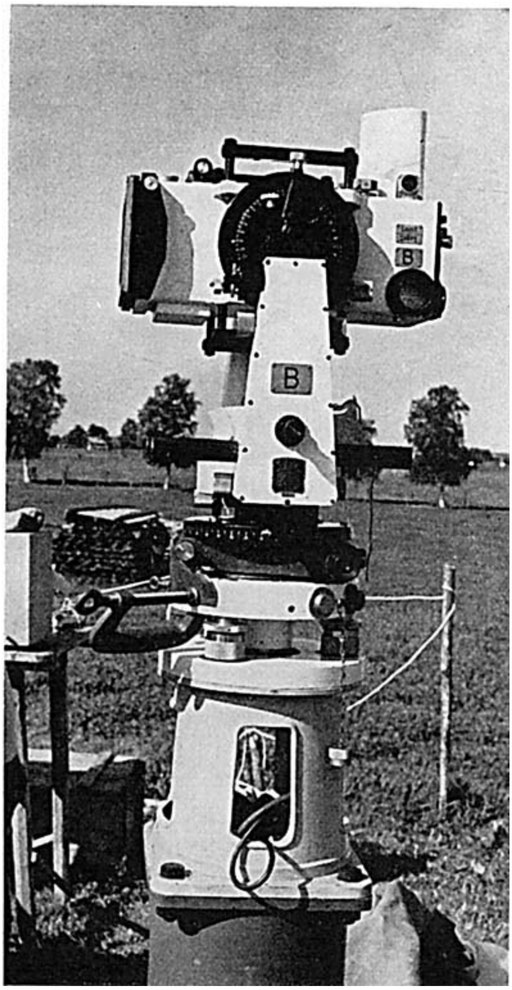

Fig. 7. Ballistic camera, set up for operation at Torsta. The instrument is mounted on a cylindrical iron pedestal set into a concrete pad. The camera constant is 378.66 mm. The *f*/5 Tessar objective is located on the right-hand side. Accurate setting of elevation angle and azimuth can be made at every 5th degree with the aid of an eyepiece on the right-hand side of the azimuth circle. A visual theodolite is included for accurate orientation of the instrument, the reference direction being marked by an illuminated signal about 2 km away. The cameras are fitted with a special device for illumination of the fiducial marks, not shown in the picture.

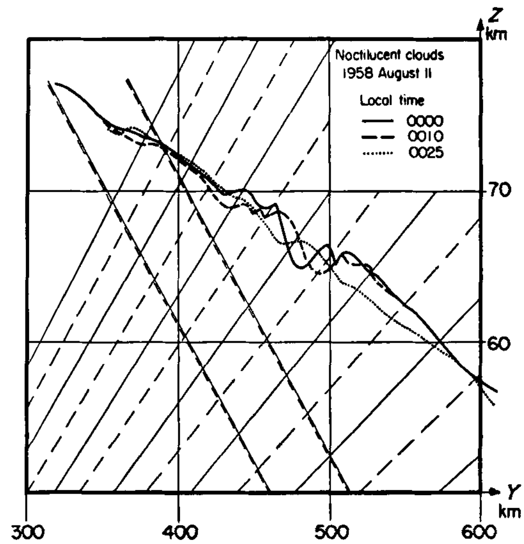

Fig. 8. Vertical cross-sections through the cloud layer in a north-south direction through the centre of the pictures in Figs. 11*a*, 12*a* and 13*b*. The horizontal coordinate is the northward distance in the plane tangent to the earth at point *B* and the vertical scale is the height above this plane, not corrected for refraction. The sloping lines indicate directions of vision at every 0.5° elevation angle. The two parallel lines are shown to indicate the geometrical shadow of the 20 km and 30 km atmospheric layers. The crest of the wave in the pictures is seen in the centre of the diagrams. The northward displacement and deterioration of the wave crest is well seen. The diagrams show also the increase of the effective optical thickness of the clouds when the line of sight coincides with the rear slope of the wave crest.

visibility was good. As the depression of the sun was favourable, 8 to 11 degrees, this display proved to be among the brightest ever seen in Sweden. The clouds were first observed about 10° over the northern horizon at 2215 local time in the form of faint remnants from a past cloud system. The clouds moved towards the south-west and eventually disappeared from the field of view. Meanwhile a second system could be observed to emerge from the horizon in the north-east. The feature first observed was a bright area, surrounded by more diffuse regions, which became more distinct with increasing solar depression. The cloud system moved rapidly towards the south-west and the development at this stage is shown in Figs. 10*a* to *d* arranged in a time-lapse sequence of ten and fifteen minute intervals. These plates were taken from point *A* with the camera axis pointing 30° east from north, elevated 10°. Apart from the successive displacements of the bright feature, the pictures show systems of billows and other small-scale irregularities which were already visible at an early stage. It should be mentioned that for some peculiar reason the

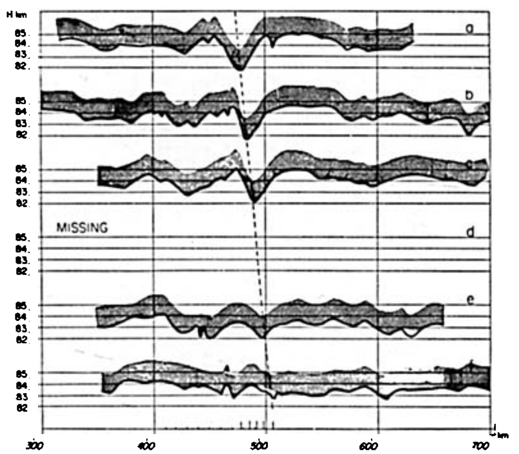

Fig. 9. Time sequence of consecutive vertical cross-sections corresponding to the pictures in Figs. 11 to 14. The vertical coordinates are the computed heights above surface level and the horizontal scale is the distance to the points at cloud level. The time difference between each diagram is 5 minutes. The solid curve indicates the bottom topography of the cloud system. Consecutive positions of the crest of the wave seen in the centre of the pictures are connected by a broken line indicating a northward displacement. The curves were obtained by connecting height values measured at fixed grid points. Thus small-scale features of the bottom topography are partly smoothed out. Beyond 600 km the measurements are less reliable. Indications of the second wave crest are seen near 600 km, as seen also on the contour maps.

cloud details are more easily perceived if the pictures are viewed upside-down. From the anaglyph picture *a* in Fig. 2, a three-dimensional view showing this development is obtained. The picture pair was taken at a time intermediate between Figs. 10*c* and *d*. The plates show also a system of parallel bright bands which appear on the cloud surface. Toward midnight the brightness of these bands apparently increased and the bands remained over the sky for the rest of the night. An interesting phenomenon is exhibited by the brightest regions to the right from the centre of the photographs where a kind of diffuse veil apparently is falling out from the cloud surface. Due to the diffuse character of the veil, good height measurements could not be obtained so far, even by the stereo method. The analysis indicated, though, that the veil was actually located below the surrounding cloud system. A possible interpretation of the phenomenon may be found in a local fall-out. At midnight the clouds were visible over an area of 60° in azimuth and about 15° in elevation and were centred at a point about 10° east of north. At this time our attention was turned to the remarkable development in the north, shown in Figs. 11–14. The seven photographs were taken from Torsta in the zero direction in consecutive five-minute intervals beginning at 0000 local time with camera elevations of 10° and 5°. The pictures should speak for themselves, although a few features of detail should be pointed out. These are (*a*) the twisting and destruction of the wave crest near the centre of the pictures, (*b*) the passing of billows and other irregularities through the same wave crest, and (*c*) a peculiar kind of granulation of certain regions best seen in Fig. 13*b*. The analysis proved, that this granulation was a regular pattern of "holes" in the cloud surface and is suggestive of convection cells. Typical dimensions of these and other irregularities will be given below. The change of position of certain darker areas may be followed from picture to picture and these regions are probably advected with the cloud system and indicate, therefore, the direction of the horizontal wind.

The small-scale features of the cloud system began to vanish slowly with increasing illumination, and later the only distinct details were the bright bands or waves previously mentioned. This stage of development is shown in Figs. 10*e* to *g* which were taken from Torsta at 0120, 0143, and 0156 local time. The plates show changes in the position of the bright bands which indicate a north-eastward displacement. The phenomenon is remarkable considering that the cloud system as an entity was travelling in the opposite direction. These bands were actually due to waves in the cloud layer which propagated in a direction opposite to the cloud movement as is shown by the analysis. Later these bands also became fainter and eventually vanished shortly after 0230. The last weak remnants of the display were observed at a very high elevation angle where they became covered by cirrus clouds. In spite of the favourable viewing conditions which remained for another night, no further traces of noctilucent clouds were detected.

The results from the photogrammetric analysis work begin with a series of vertical cross-sections through the cloud layer, shown in

2 a.

2 b.

Fig. 2. Anaglyph pictures showing parts of the display of August 10–11, 1958. The photographic pairs printed together were taken from the endpoints of the Torsta base line (length 51.5 km). The pictures should be viewed through the coloured glasses attached to this issue. The blue glass should cover the right eye. The pictures should be held at normal distance of about 25–35 cm, with the eye accommodated to infinity. *After a few seconds a threedimensional view of the cloud system is obtained.* To emphasize this effect an arrow is printed on one of the pictures. The pictures can be viewed upside-down in which case the glasses must be turned.

Picture *a* was taken in a direction 30° east from north at an elevation angle of 10° at 2330 local time and picture *b* at 0010 in direction north, the elevation angle being 5°. The exposures were 5 sec on Kodak P1200 emulsion. Features to be noticed in *a* are the parallel bands corresponding to waves in the cloud surface, the billow system in the left centre and the veil of diffuse matter, apparently falling out from the cloud.

In *b* the system of parallel waves is seen even better. The system of waves propagated in a direction opposite to that of the cloud system as a whole. The smaller-scale irregularities followed the cloud system in its movement toward the southwest.

Fig. 12 a. 00.10

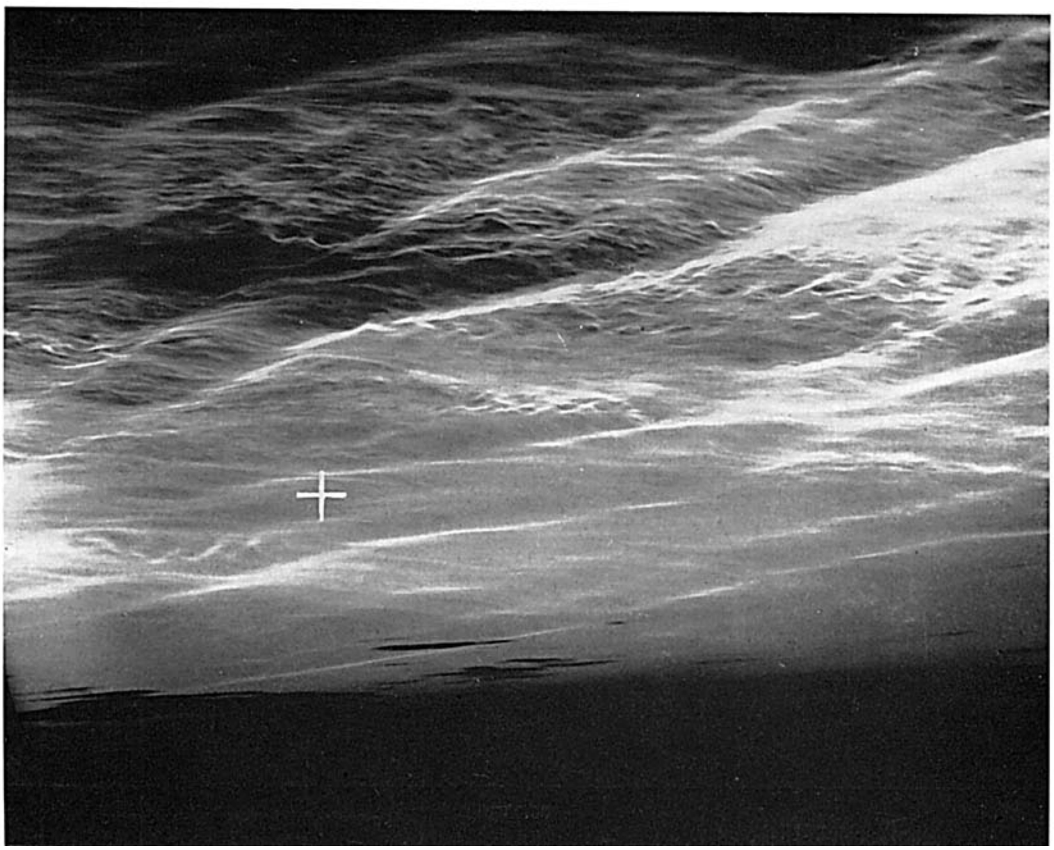

Fig. 12 b. 00.15

Fig. 13 a. 00.20

Fig. 13 b. 00.25

Fig. 14. 00.30

Figs. 11–14. Time sequence showing the display on August 10–11, 1958. Photographs made from Torsta at azimuth 0° north with exposure times of 8 and 12 sec. For pictures 11*a* and *b* the elevation angle is 10°, and for the others 5°. The pictures are of original size and the centre is marked by a cross. Held upside-down the pictures give an impression of perspective. Times are indicated below the pictures in local time. The bright line in the centre of the pictures is due to a wave whose structure is seen from the contour maps in Figs. 15 to 17. The wave, which is seen to be refracted, propagates towards the north-east with a speed of about 10 m/s, against the movement of the cloud system it self. An area containing billows (right from centre) can be seen to catch up and pass the wave crest (13*a*). Close examination of picture 13*b* reveals a sort of granulation due to apparent "holes" in the cloud surface. This structure is shown in Fig 32. The dark region seen in the middle of picture 12*a* and displaced to the left in the later pictures may be caused either by a local decrease in the particle density or as an effect of the geometry of the cloud.

Fig. 19. Enlarged picture from the central portion of picture 11*b*, showing the cloud surface between the two nearest waves.

Fig. 8. These cross-sections were made in a north-south direction through the centres of Figs. 11*a* and *b*, and 12*a*. The horizontal coordinate is the distance Y measured northward in the plane tangent to the earth at point B. (the height of point B is about 400 m above sea level). The vertical scale is the measured height Z above this plane without correction for atmospheric refraction. Distances are indicated in kilometers. The contour lines were drawn partly by the map-drawing apparatus previously described and partly by connecting height values measured at fixed grid-points 5 and 10 km apart. The wave profile corresponding to the bright band at the image centre is well marked. The curves also illustrate the northward displacement of the intersection of the wave profile with the zero direction. Sloping straight lines indicate directions of vision at different elevation angles. The cause of changes in the brightness of the clouds with the viewing direction may be explained by a study of the intersection of these lines with the cloud surface. The intensity of light scattered by particulate matter is known to be proportional to the number of particles in the line of sight. The cloud layer is of finite depth and the effective optical thickness will vary with the angle between the cloud surface and the line of sight. This is seen in the diagrams of Fig. 8. Thus dark portions in the picture correspond to the front slope and the bright bands to the rear slope of actual waves in the cloud surface. It should be noticed that the cloud surface throughout the wave is continuous. This indicates that local increase of the particle concentration, due for instance to a condensation process, is not necessary for the explanation of the band structure. This is true not only for long waves but also for other features since brightness changes can be expected from any kind of inclination of the cloud surface to the line of sight. If the wave is steep or if irregularities appear superposed on the crest, brightness may change by a factor of the order of ten or even more. This is a plausible explanation of the fact that the bright bands are the only details observed when the contrast is weak or the visibility poor. LUDLAM (1957) has proposed a similar mechanism as being responsible for brightness differences. The effect is there ascribed to waves in a haze top. Another phenomenon is described in the same paper in the following way: "Except in very intense displays, the clouds have been seen more often after than before midnight, even though the number of observers is likely to be less at the later hours". Now these more recent observations indicate that the waves first appear at a later time. The above phenomenon could be explained by the optical effects caused by the waves if these are actually absent or weakly developed during the earlier stage of a display. A second type of vertical cross-sections is shown in Fig. 9. The horizontal coordinate is the northward distance at cloud level. This is approximately equal to Y. The vertical axis is the height above surface level H. The cross-sections are made as before through the image centre in a north-south direction and distances are in kilometers. The heights were measured at the lower boundary of the cloud features. Thus the curves show the bottom topography of the cloud layer. Attempts to measure the vertical extent of the cloud details were made only in a few cases. Since the heights are measured at fixed gridpoints, irregularities of a scale smaller than the mesh width are partially smoothed out. Locally the actual maximum height values may exceed those values indicated here. The cross-sections were made from Figs. 11–13, picture 12*b* having been rejected because of a broken plate. They clearly demonstrate the wave structure of the cloud surface. It is observed that the mean height of the cloud surface was nearly constant over long distances. It should be noticed though that at distances beyond 600 km the measurements become less certain due to the confluence of cloud details. The main feature is the wave in the centre of the photographs. Consecutive positions of the crest of this wave are connected by a broken straight line. Since time differences between the cross sections are constant, this line may be used together with the length scale at the bottom of the figure to estimate the propagation velocity of the wave front. The intersection of the wave crest with the zero line is found to travel northward with an average speed of about 20 meters per second. The true wave speed may be computed by multiplying this value by the sine of the angle of inclination between the wave front and the zero line. From the contour maps in Figs. 15–17 this angle is found to be approximately 30°. Thus the wave speed is about 10 m/s. At this point the direc-

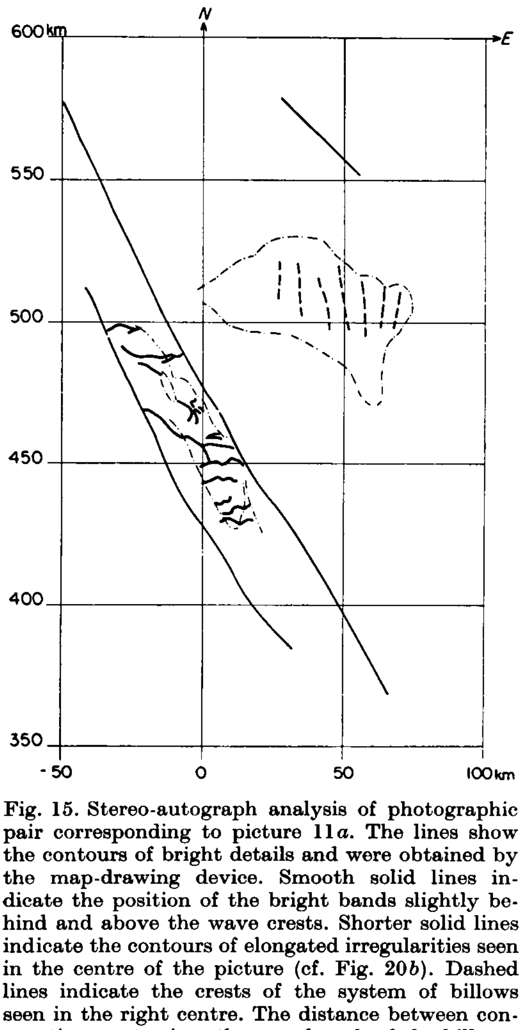

Fig. 15. Stereo-autograph analysis of photographic pair corresponding to picture 11*a*. The lines show the contours of bright details and were obtained by the map-drawing device. Smooth solid lines indicate the position of the bright bands slightly behind and above the wave crests. Shorter solid lines indicate the contours of elongated irregularities seen in the centre of the picture (cf. Fig. 20*b*). Dashed lines indicate the crests of the system of billows seen in the right centre. The distance between consequtive crests gives the wavelength of the billows, 6 to 9 km. Dot-dashed lines show the boundaries of diffuse areas surrounding and covering the billows. Greatest measured height is 85.5 km in the vicinity of the uncovered billows. Height of the bright bands about 82.5 km.

tion of propagation is approximately 60° east from north. The maximum amplitude of the wave is found to be about 3 km. It must be pointed out that this wave seems to represent an extreme case; amplitudes of 1.5 to 2 km were measured more generally. From the diagrams we might also determine the distance between consecutive wave crests. This is, however, more readily made from the contour maps.

The contour maps are shown in Figs. 15–17. They correspond to Figs. 11*a* and *b*, 12*a* and 13*a* and *b*. The reader is advised to view the maps together with the corresponding pictures. Except for the first map in Fig. 15 the contour lines were obtained from an analysis of height values measured at fixed grid-points. The grid size was 5×5 km and 10×10 km farther out from the centre. In the vicinity of particularly interesting details the grid size was even smaller. Such details are shown in Figs. 21, 22 and 23. The grid size is here 1.25×1.25 km, and 2.5×2.5 km. The isopleths are lines for constant height given for 500 meter intervals. Increasing height is indicated by shades of increasing darkness. Regions above 85 km are black. The coordinate system is the $X-Y$ system defined in the previous section. This is not a true projection although in the region considered the differences between distances in the $X-Y$ plane and true distances at cloud level are small. The system has been chosen in order to take advantage of the map-drawing apparatus previously described. Thus contour lines and boundaries of a variety of cloud features could be drawn directly. Short solid lines obtained in this way indicate elongated, small-scale irregularities with characteristic sizes of the order of a few hundred meters. Contours of droplet-shaped or circular features are represented by closed solid curves while crests of billow-type corrugations are indicated by thick broken lines. In some of the maps the crests of the longer waves are also indicated. The map in Fig. 15 was entirely drawn by the map-drawing device. Here the long solid lines which indicate the waves were obtained as the measuring mark followed the bright lines seen in the photographs and do not coincide with the actual wave crests. Similar lines in the analyzed height maps were as expected, located slightly behind and above the wave crests. Part of the cloud system seen in the photographs is covered by more diffuse matter. Boundaries of such areas are indicated by thin dot-dashed lines. Relative height differences between adjacent points were within the limits of the estimated accuracy and the measurements were reproducible. At distances beyond 600 km and near the edges of the plates the accuracy is less. The variation in the average height of the cloud surface from picture to picture is of the order of ± 500 m. The individual heights were found to vary from about 81.10 to 85.5 km. These values apply to the bottom topography of the well

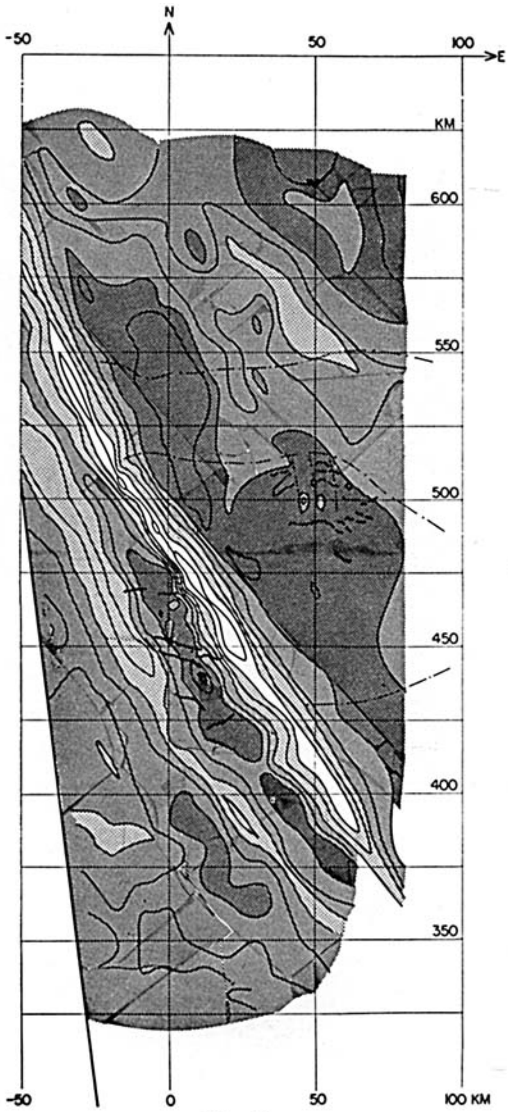

Fig. 16 *a*.

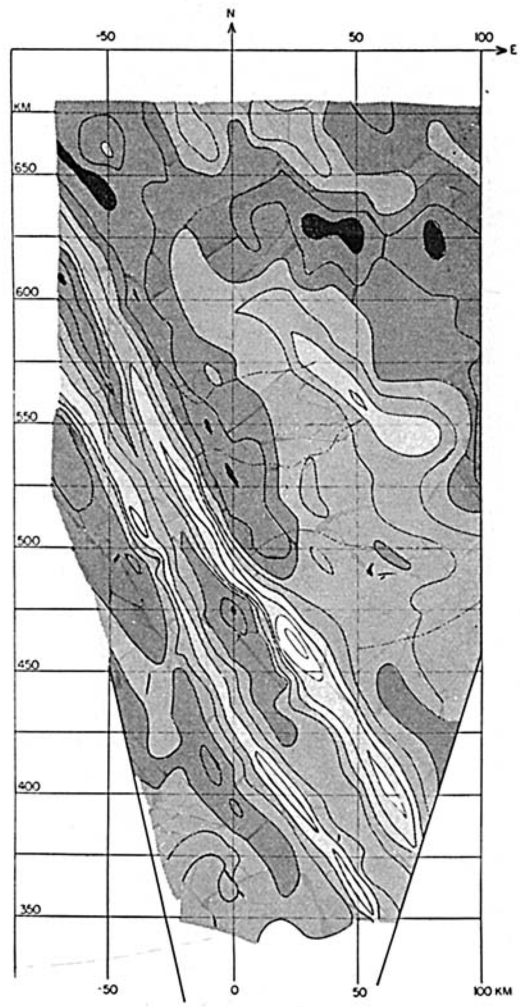

Fig. 16 *b*.

Figs. 16–17. Contour maps obtained from analysis of height values measured at fixed grid-points. The coordinate system is the $X-Y$ system which is not a true projection. The isopleths are spaced at equal 500 m height differences. Areas higher than 85 km are black while those below 82 km are white. Straight solid lines indicate the limits of the field of view in the photographic pair. Fig. 16*a* corresponds to Fig. 11*b*. Short solid lines indicate the contours of elongated irregularities passing between the two waves. (See also Fig. 20*a* and *b*.) Broken lines indicate as before billow crests and dot-dashed lines show the boundaries of diffuse regions. Indications of a wave parallel to those in the centre are seen in the upper part of the map. Fig. 16*b* corresponds to Figs. 12*a* and 2*b*. The northward displacement of

defined cloud layer. Veils of more diffuse matter below this layer are locally observed. Attempts were also made to measure the vertical extension of irregularities by letting the measuring mark of the analyzing instrument penetrate the cloud layer. Heights up to 86–87 km were obtained in this way. These values, which also apply for instance to details covered by small-scale irregularities, are obviously less accurate. It should be noted that only part of the details

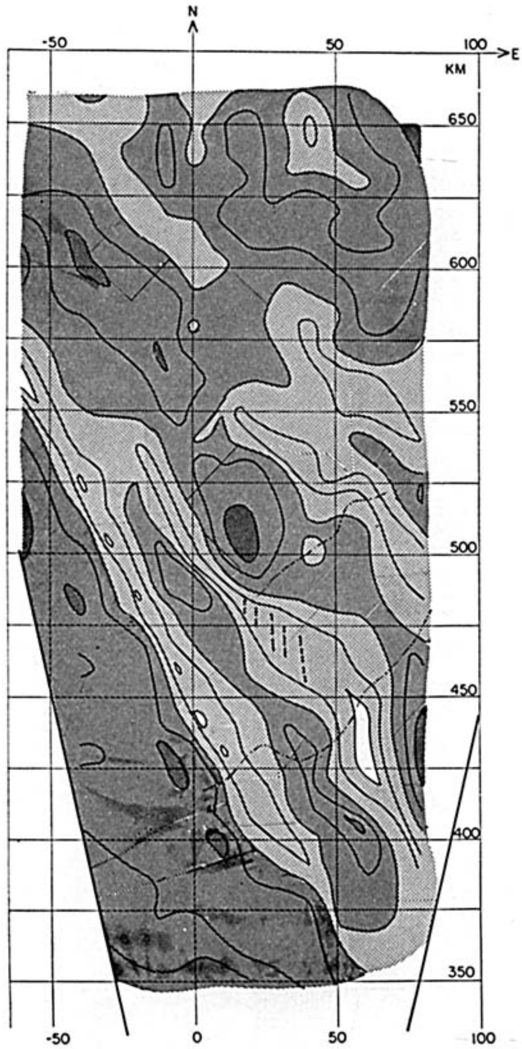

Fig. 17 *a*.

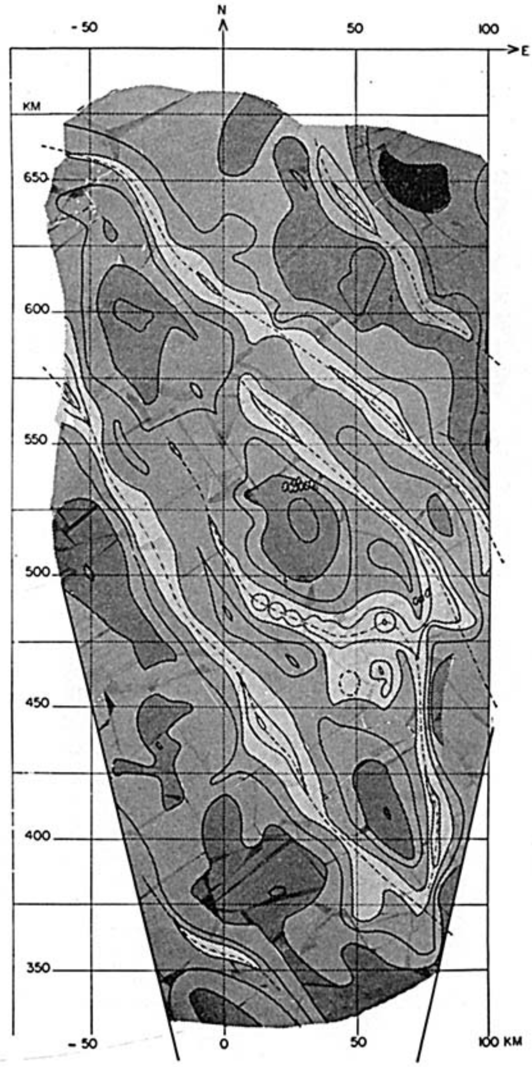

Fig. 17 *b*.

the waves in the centre is clearly seen, as well as the signs of refraction of the preceding wave. Fig. 17*a* corresponds to picture 13*a*. Short broken lines are crests of billows passing through the longer wave. The waves are displaced further north-eastwards and the refraction is seen to proceed. Fig. 17*b* corresponds to picture 13*b*. Here, the broken lines follow the wave crests to emphasize the wave structure. The granulation observed in the picture is illustrated by the small closed curves in the centre, obtained with the map-drawing device directly from the stereo-autograph. (See also Fig. 23.) Contours of droplet-shaped irregularities can be seen on the crest of the refracted wave. The waves propagate as before.

in the photographs are covered by the present analysis. Various particular features have been studied in different picture pairs but only the contours of a few outstanding details are indicated in the maps.

The analysis indicates that the cloud system consisted of a practically continuous layer of particles exhibiting a more or less regular pattern of deformations of various sizes. The most interesting of these deformations is a system of parallel crests evidently associated with a form of wave motion. The waves are observed to propagate in a north-easterly direction. The sequence of maps shows the refraction of one of the wave crests. The characteristic wavelength, defined as the shortest distance between adjacent crests, is found to vary from 30 to 40 km. Similar values were also obtained by analysis of other picture pairs, particularly that shown in Fig. 10*d*. In some parts of the cloud system the wavelength is seen to attain values of about 75 km, which would be twice as large as above. This, though, might be due to the impossiblity of identification of a missing crest. Consecutive displacements of the wave crests indicate the speed of propagation of the waves relative to a fixed frame of references, as illustrated by Fig. 18. This diagram shows the position of the waves at different instants. Time differences are constant so that the length of arrows connecting the crests belonging to one and the same wave indicates the speed of propagation. The average velocity measured in this way is 10 to 15 m/s directed north-easthward. This is practically opposite to the direction of the mean air flow which carries the cloud particles. The contour maps show point-to-point variations in the wave velocity, particularly in the region where the strong refraction is observed.

The speed of the mean horizontal flow could not be determined with certainty. Estimates could be made, however, by studying consecutive displacements of bright areas, such as shown in Figs. 10*a* to *d*, as well as movements of certain other well-defined irregularities. Wind speeds of 80 to 120 m/s were obtained with the aid of the bright spots which were observed at an early stage of the display. In the second case which refers to the area shown by the contour maps wind speeds of 60 to 80 m/s were found. Variations of the wind velocity in both space and time are likely to be expected. With these values, the true wave velocity with respect to a frame of reference moving with the cloud system becomes 70 to 135 m/s.

The average amplitude of the wave is about 2 to 3 km, although locally larger height differences can be found. Thus, for instance, small-scale irregularities passing through the wave crest may increase the apparent depth of the wave. In certain regions the apparent height gradient of the cloud surface is found to be

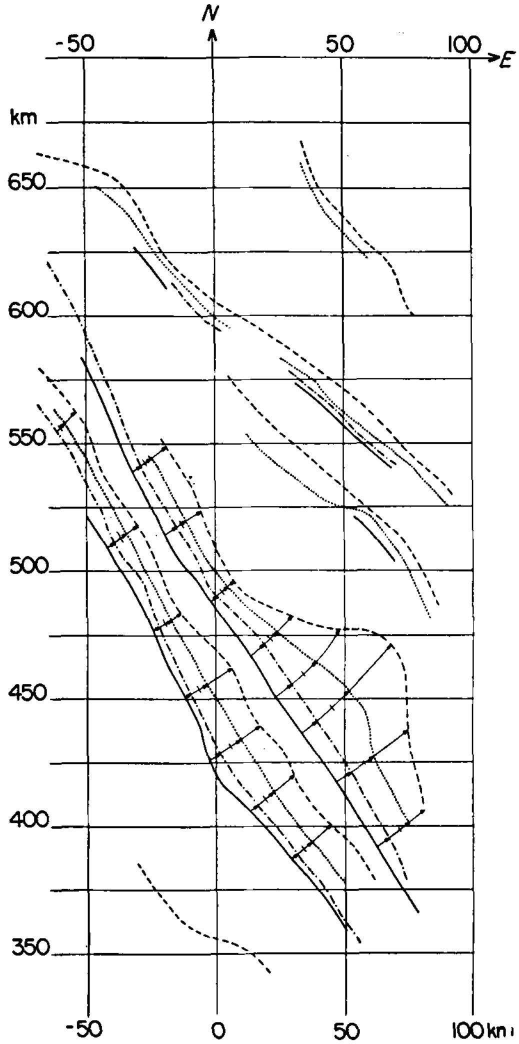

Fig. 18. Displacement of the wave crests. Consecutive positions of the wave crests in Figs. 16 and 17 are copied together on this diagram. The coordinates are as before. Solid lines indicate the position of the waves at time 0000, dot-dashed lines at 0005, dotted lines at 0015 and dashed lines at 0020. Due to the constant time differences the arrows connecting the waves indicate the direction as well as the magnitude of the propagation velocity. Remarkable is the difference in speed between various points along the refracted wave. It should be pointed out that the cloud system as a whole moved in a direction opposite to the waves. The average wave speed is about 10 m/s.

very large. Such a region is shown by the enlarged photograph in Fig. 19 and the corresponding detailed analysis in Fig. 20. Where the maximum slope is about 45 degrees. This should

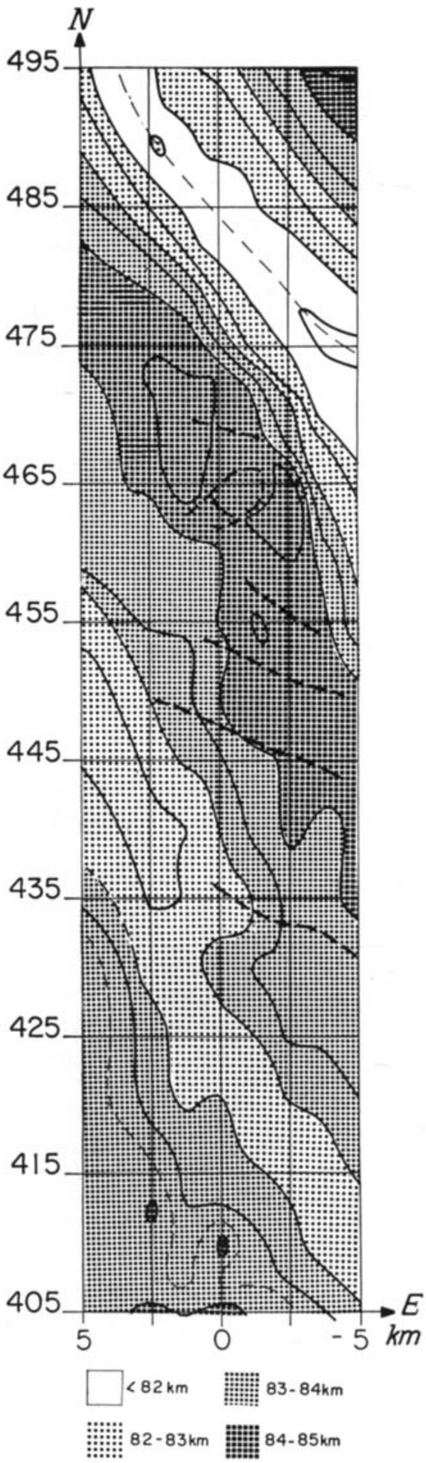

be regarded as an extreme case presumably due to a local change in the horizontal wind speed versus the wave velocity. More moderate variations of the height in the vicinity of the waves are found in similar maps in Fig. 22 and 23.

Discussion

The appearance of the pattern suggests that the paths of the cloud particles follow the observed cloud surface. If this is true, then the measured height differences are approximately equal to the vertical amplitude of the trajectories. If the waves are due to a sinusoidal oscillation in a vertical plane, it may be shown that the amplitude of the vertical motion W is connected with the wavelength L, the horizontal propagation velocity C, the speed of the basic flow U and the height difference H by the relationship

$$W = 2\pi(U - C)H/L,$$

where $U - C$ is the velocity of the wave with respect to the moving air. With $L = 40$ km, $(U - C) = 80$ m/s and $H = 2$ km we obtain $W = 25$ m/s. Although this value might appear somewhat excessive the order of magnitude seems to be correct. It is furthermore considerably larger than the terminal fall velocity of particles of the size range found in noctilucent clouds. Thus the fall velocity may be neglected in the discussion of the wave motion. Computed from a gas-kinetic formula applying to the case of particle dimensions smaller than the mean free path of the air molecules (KENNARD, 1938, p. 310) the terminal fall velocity of particles with 0.1×10^{-4} cm radius is about 50 cm/s at the 85-km level.

The waves are oriented nearly perpendicularly to the mean air current. Weak indications of periodic height variations in other directions

Fig. 20. Contour map of the portion of the clouds seen in Fig. 20. The height values were measured at gridpoints 1250 m apart. The solid lines are isopleths given for 500-meter intervals. Short dashed lines indicate smaller-size irregularities while a thin broken line indicates the crest of the wave. The diagram shows a tremendous height gradient across the wave. The wave appears to be retarded in this region. Thus, the appreciable steepening of the slope of the wave may be associated with local changes in the wave velocity versus the air flow. It should be noticed that the diagram gives a smoothed picture of the cloud surface as the maximum and minimum heights are not indicated.

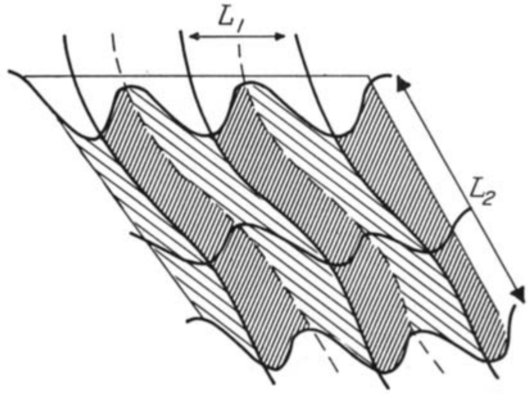

Fig. 22. Schematic presentation of billow-type corrugation of the sort indicated in the contour maps. The wave pattern is often twodimensional as found from height measurements at closely spaced points. This type of wave pattern was always found to propagate in the same direction as the movement of the cloud system. The wave normals of some billow systems are oriented nearly parallel to those of the longer waves while in other cases an inclination of up to 45° to the main flow is found. The characteristic wavelengths L_1 and L_2 vary from about 4 to 9 kilometers; the amplitudes between 500 and 1000 meters.

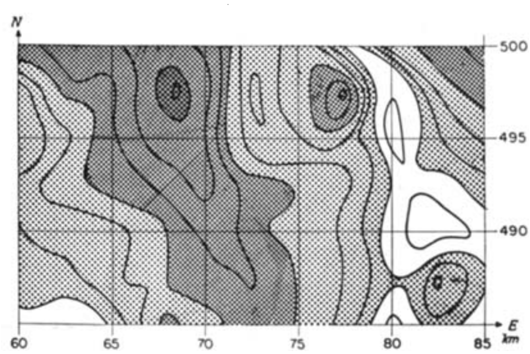

Fig. 23. Detailed study of a portion of picture 13*b* illustrating the peculiar granulation observed in the picture. The interval between isopleths is 200 m. Darker shading indicates heights about 83 km while those below 82 km are white. The region shown here is also located between the two nearest waves. Although represented by closed curves, it seems likely that the phenomenon is due to closely spaced small-scale irregularities of droplet shape.

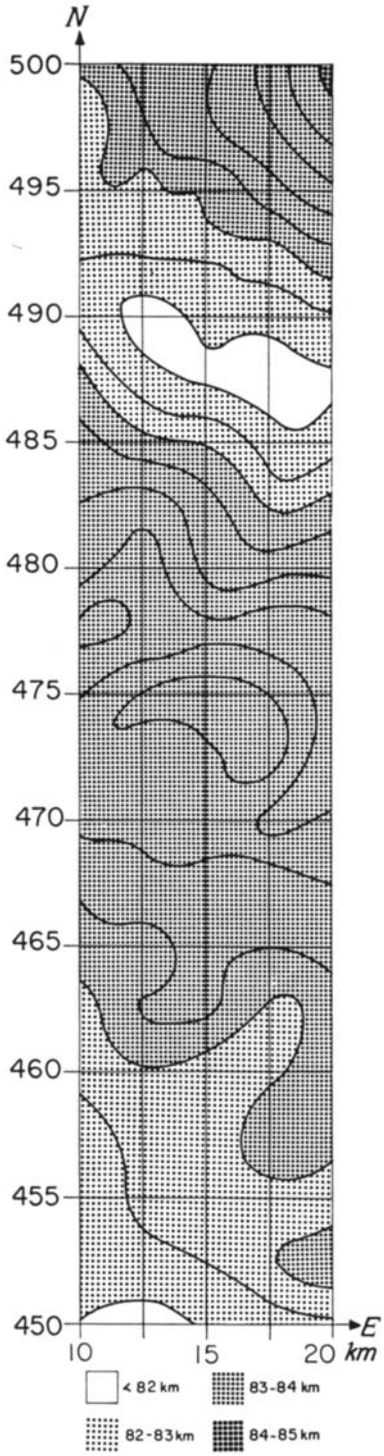

Fig. 21. Contour map of part of the central portion of picture 13*b*. The region shown is similar to that in the previous figure. The isopleths are here given for 200 m intervals and the spacing of grid-points is 2.5 km.

were also observed. This has been confirmed by time-lapse films taken from more recent displays.

The origin of the wave motion is not known so far. It appears reasonable to assume that they belong to the type known as internal gravity waves modified by a possible wind shear. Neither the speed nor the direction of propagation contradicts this hypothesis. The existence and properties of such waves in the upper atmosphere have recently been discussed by HINES (1959 and private communication). It can be shown (QUENEY, 1947) that internal gravity waves can exist in the atmosphere with frequencies satisfying the relationship

$$\omega < \omega_s = \sqrt{gs},$$

where s denotes the static stability defined by

$$s = 1/T\left\{\frac{\partial T}{\partial z} + g/c_p\right\}.$$

T is here the absolute temperature and g and c_p denote the gravitational constant and the specific heat at constant pressure, respectively. Observational data are too scarce to use a theory to fit the observations. The properties of these waves can, however, be illustrated by a very much simplified model. Assume for instance a purely two-dimensional vertical oscillation in a constant basic horizontal flow of velocity U and neglect the fall velocity of the particles which thus are assumed to be advected with the air. Neglect also the rotation of the earth and the wind shear. The frequency of this oscillation becomes

$$2\pi(U-C)/L,$$

where C is the observed propagation velocity. Taking as an example a wave where $L = 40$ km and $(U-C) = 80$ m/s we have $\omega = 1.26 \times 10^{-2}$ while, assuming isothermal conditions at $T = 160°$K,

$$\omega_s = 2.5 \times 10^{-2}.$$

This model is obviously very crude and a complication might arise from a possible failure of the perturbation analysis of these waves due to the large vertical amplitudes. These considerations show also that a gravity oscillation wavelength of the scale observed, will necessarily imply a large propagation velocity. If the latter exceeds the drift velocity such waves will be observed to move against the wind.

Wave motion on a smaller scale is represented by systems of parallel billows of different orientations. The appearance of the billows may remind an observer of that of tropospheric clouds or a "mackerel sky", as sometimes seen in literature. Analysis shows that, at least in this case, the cloud surface was continuous between the billow crests. The structure of the billows is shown in a schematic drawing in Fig. 22. Thus, it is reasonable to conclude that the increased brightness of the crests is due to geometrical effects rather than to a sublimation- and reevaporation process (see Fig. 8). The characteristic wavelength of the billows is about 4 to 9 km with amplitudes of about 500 to 1000 m. The orientation of the billows in one and the same system compared to that of the longer waves is an interesting feature. In some cases the wave normals of the two systems were found to be nearly parallel while other billows exhibited deviations of up to 45 degrees. The different orientations may indicate a possible change with altitude of the direction of the horizontal flow. Certain billows with crests oriented parallel to the mean flow have been observed to form an almost standing wave pattern. Billows parallel to the longer waves were observed to propagate in the same direction as the cloud system, although the velocity of propagation probably is different from that of the basic flow. The billows are observed to pass through the crests of the longer waves.

If we assume the billows to be similar in nature to the longer waves, we may use the previous considerations to obtain an idea about the order of magnitude of the velocities involved neglecting as previously the vertical shear. If the frequencies of the two oscillations are the same, then the ratio of propagation velocities is equal to the ratio of the wavelengths, or

$$(U-C_1)/(U-C_2) = L_1/L_2.$$

With $L_1 = 40$ km, $L_2 = 7.5$ km and $U - C_1 = 80$ m/s, we have $U - C_2 = 15$ m/s. With $C_1 = 10$ m/s, we obtain $U = 70$ m/s and $C_2 = 55$ m/s. The speed and direction of the propagation are again consistent with observational facts. This shows also that the error introduced by using the motion of the billows for an estimate of the horizontal wind speed is fairly small and can be further reduced by also taking the motion and length of the longer waves into account. Displacements of the longer waves, which on occasion are the only features observed in a display, indicate the horizontal wind only if a certain period of oscillation is assumed. An interesting implication is that if the horizontal flow were measured independently, for instance by a rocket technique, the ratio of periods of the two oscillations could be found.

The last feature to be pointed out is the peculiar pattern of apparent holes in the cloud surface. Fig. 23, which is a detailed analysis of part of Figs. 13*d* and 17*b*, illustrates this phenomenon showing the contours of some of the elements in this pattern. Since the cloud surface is seen under a low angle of inclination, the vertical extension of the holes could not be measured. It was therefore impossible to determine whether the hole were caused by a form of cellular convection or by superposition of a small-scale mamato pattern of falling particles in the line of sight. The resolution of the photogrammetric analysis also limits a more accurate analysis of features of this scale because of the high speed of the movement of the clouds which in combination with the 10-second exposure time tends to smear out the boundaries of the pattern. The phenomenon is nevertheless real and the scale shown in Fig. 23 is reasonably accurate. Small-scale turbulence might be a possible explanation for the hole pattern as well as for a variety of irregularities of comparable sizes.

Remarks

The analysis of the structure of noctilucent clouds presented above will possibly contribute to the knowledge of dynamic processes in the vicinity of the mesopause. The results leave the field open for speculations concerning the origin and generation of the different wave motions involved. It might be pertinent to mention here the work of Palm and Foldvik (1960) on mountain waves. The authors show that under certain conditions a local disturbance at lower levels may set up wave motions with a wide range of wavelengths, extending to fairly high elevations. The observations indicate that a sublimation-and-reevaporation process as a cause of wave formations is not absolutely necessary for the explanation of the observed features. Moreover, sublimation processes at high altitudes have recently been discussed from the thermodynamical point of view by Hesstvedt (1961) who concludes that a plausible value for the growth rate of particles in the size range considered is 0.004×10^{-4} cm increase of radius per minute. It is evident from the observations that the particles move through one single wave in only a few minutes. Thus, it appears unlikely that with a growth rate of the same order as mentioned above an appreciable change in size can take place to account for the differences in optical density within the observed pattern. We can thus account for the appearance of waves and billows from purely geometric reasoning and need make no assumptions about changes in particle size. This does not exclude the possibility that the cloud layer itself might be formed by sublimation of water vapour on suitable nuclei. Small particles will spend sufficient time in the cloud layer as a whole so that the growth to the size observed could easily take place. There is an essential condition, though, that the temperature of the air and the particles is sufficiently low with respect to the available humidity to produce the required supersaturation. The presence of a concentration of solid particles near the mesopause has been well established. The very low summer temperatures at the levels and latitudes in question have been established by rocket investigations (Stroud *et al.*, 1960). The present knowledge of the abundance of the H_2O molecule at high altitudes is unfortunately scarce and theoretical discussions are restricted to values extrapolated from measurements in the middle stratosphere. To gain a further insight into the nature of noctilucent clouds, it would be necessary to know about the actual physical conditions in and around the clouds themselves. Such knowledge demands a complex programme of physical measurements at the times and in the regions where the clouds are known to occur. The measurements should be made when the clouds are visible as well as when they are not. A possible combination of such measurements with a technique for sampling and microanalysis of the cloud particles would be of great value. We hope that increased activity in the field of rocket research in Sweden and elsewhere will bring about a definite solution of the problem of noctilucent clouds.

REFERENCES

Burov, M. I., 1959, Fotogrammetrichessky metod opredelenia serebrystih oblakov. *Trudi Sovesh-chanya po Serebristim, Oblakam, Tartu.*

Hesstvedt, E., 1961, Note on the nature of noctilucent clouds. *J. of Geophys Res.*, **66**, pp. 1985–87.

Hines, C. O., 1959, An interpretation of certain ionospheric motions in terms of atmospheric waves. *J. of Geoph. Res.*, **64**, pp. 2210–2211.

Jesse, O., 1896, Die Höhe der Leuchtenden Nachtwolken. *Astr. Nachr.*, **140**, pp. 161–168.

Kennard, E. H., 1938, *Kinetic Theory of Cases.* McGraw-Hill Book Comp. Inc., p. 310.

Khvostikov, I. A., 1952, Serebristye Oblaka. *Priroda*, **5**, No. 49.

Ludlam, F., 1957, Noctilucent clouds. *Tellus*, **9**, pp. 341–364.

Palm, E., and Foldvik, A., 1960, Contribution to the theory of two-dimensional mountain waves. *Geof. Publikasjoner* **21**, No. 6.

Paton, J., 1949, Luminous night clouds. *Met. Magazine*, **18**, p. 354.

Queney, P., 1947, *Theory of Perturbations in Stratified Currents with Application to Air Flow over Mountain Barriers.* Miscellaneous Reports No. 23, University of Chicago.

Stroud, W. G. *et al.*, 1960, *Rocket Grenade Measurements of Temperatures and Winds in the Mesosphere over Churchill, Canada.* Space Research, Proceedings of the First International Space Science Symp. Ed. by H. Kallmann Bijl. North Holland Publ. Comp. Amsterdam, pp. 117–143.

Størmer, C., 1935, Measurements of luminous night clouds in Norway 1933 and 1934. *Astrophysica Norvegica*, **1**, No. 3.

Witt, G., 1957, Observations of noctilucent clouds. *Tellus*, **9**, pp. 365–371.

Witt, G., 1960, Polarization of light from noctilucent clouds. *J. of Geophys. Res.*, **65**, pp. 925–933.